Optics Letters

Nonlinear distortion mitigation of DML-based OFDM optical systems with non-orthogonal DFT-precoding

Peiji Song,[1] Zhouyi Hu,[2,*] Yizhan Dai,[1] and Chun-Kit Chan[1]

[1] Department of Information Engineering, The Chinese University of Hong Kong, China
[2] Department of Electrical Engineering, Eindhoven University of Technology, 5612 AZ Eindhoven, Netherlands
*z.hu@tue.nl

Received 24 May 2023; revised 28 July 2023; accepted 4 August 2023; posted 9 August 2023; published 29 August 2023

We propose a non-orthogonal discrete Fourier transform (DFT) matrix precoding scheme for the mitigation of nonlinear distortion induced by the interaction between laser chirp and fiber dispersion in a directly modulated laser (DML)-based orthogonal frequency division multiplexing (OFDM) transmission system. Compared with conventional OFDM, the proposed method can decrease the peak-to-average power ratio (PAPR) and significantly reduce the nonlinear distortion without sacrificing spectral efficiency (SE). The cascaded binary-phase-shift-keying iterative detection (CBID) algorithm is used to eliminate the inter-carrier interference (ICI) that is purposely induced by the non-orthogonal precoding. The performance of the proposed scheme is experimentally evaluated, achieving ~0.4-dB sensitivity improvement at the KP4-forward error correction (FEC) threshold over the *T*/2-spaced third-order Volterra nonlinear equalizer (VNLE). Meanwhile, compared to the VNLE, the reduction in computational complexity of one OFDM frame is 90% for multiplication and 88.32% for addition in this work.

https://doi.org/10.1364/OL.496312

The intensity modulation and direct detection (IM/DD) optical system has been extensively studied due to its low cost and complexity [1–3]. To further reduce the cost and complexity, a directly modulated laser (DML) is preferred over the schemes using additional external modulators, such as electro-absorption modulators and Mach–Zehnder modulators (MZMs) [4,5]. With the merits of flexible modulation and high resilience to fiber chromatic dispersion (CD), the orthogonal frequency division multiplexing (OFDM) technique has recently attracted considerable attention and has been applied to DML-based optical communication systems for practical applications [6–8]. However, DML suffers from strong frequency chirp, which induces severe nonlinear distortion when interacting with the CD. Previous approaches to nonlinear distortion mitigation include subcarrier-to-subcarrier intermixing interference (SSII) cancellation [9] and Volterra nonlinear equalizers (VNLEs) [10]. However, they have either limited performance or high complexity. A gapped-OFDM technique [11] leveraging a frequency gap between the direct current (DC) component and the transmitted subcarriers was proposed to avoid much of the in-band nonlinear distortion, enhancing the signal-to-noise ratio (SNR) performance in the high-frequency band. Nonetheless, it leads to a loss of spectral efficiency (SE) due to the forbidden subcarriers. Though the bit loading (BL) algorithm applied to the rest of the subcarriers can improve SE [11], it inevitably causes high complexity and round trip delay.

In this Letter, we extend our previous work [12] to employ the gapped-OFDM technique, where the BL is replaced with the recently proposed non-orthogonal discrete Fourier transform precoding (NODFT-p) [13]. Different from the scheme in [13], the pre-coded subcarriers are allocated in the high-frequency band to generate the required frequency gap. In addition to reducing the in-band nonlinear distortion, it does not sacrifice the SE and can decrease the peak-to-average power ratio (PAPR) compared with the conventional OFDM signal. With this proposed method, we have experimentally demonstrated 9.5-Gb/s QAM-4 optical signal transmission over a 100-km standard single-mode fiber (SSMF) using a DML. The results show that the proposed NODFT-p gapped-OFDM signal achieves ~0.4-dB sensitivity improvement at the KP4-forward error correction (FEC) threshold over the $T/2$-spaced recursive least square (RLS)-based third-order VNLE. Meanwhile, compared to the VNLE in this work, the computation complexity reduction of one OFDM frame is 90% for multiplication and 88.32% for addition.

Figure 1(a) shows the SNR profile of the conventional OFDM signal (230/512) after 100-km SSMF transmission under different bias currents. It can be found that the SNR distribution varied with the bias current. Specifically, the SNR of subcarriers close to the DC component (subcarrier index $\lesssim 50$) decreased as the bias current increased, while the SNR of high-frequency subcarriers (subcarrier index $\gtrsim 50$) was just the opposite. This is because the transient chirp exhibits a lowpass-filter-like frequency response whereas the adiabatic chirp shows a bandpass-filter-like response when considering the effect of CD [14]. Besides, increasing bias current can enhance adiabatic chirp while suppressing the transient chirp, thus leading to the above observations. Except for this, the relaxation oscillation frequency which increases with the bias current also causes the improvement in high-frequency SNR [6]. Since the nonlinear distortion induced by the interaction between laser chirp and fiber dispersion is mainly distributed in the low-frequency band, discarding the subcarriers near DC can help improve the overall performance, but at the expense of SE [11].

Figure 1(b) illustrates the principle of the proposed NODFT-p gapped-OFDM to eliminate the nonlinear distortion distributed

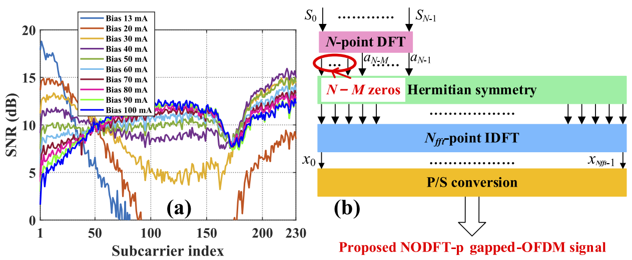

Fig. 1. (a) SNR at various bias currents in a 100-km SSMF transmission system, and (b) principle of the gapped-OFDM.

near the DC component and keep the SE unchanged. It should be noted that the gapped structure can only work effectively with the bias current ≥ 60 mA since the SNR at high frequency is good enough for transmission and is larger than that at low frequency under this case based on Fig. 1(a). Assuming that the number of subcarriers utilized by the conventional OFDM is N, for the conventional gapped-OFDM, only M subcarriers $\{a_{N-M}, a_{N-M+1}, \ldots, a_{N-1}\}$ carry the symbols [11], leaving the $(N-M)$ subcarriers $\{a_0, a_1, \ldots, a_{N-M-1}\}$ near the DC component as the gap width, where the low-frequency subcarriers are corresponding to the two edges of the inverse discrete Fourier transform (IDFT) in Fig. 1(b) [15]. However, for the proposed NODFT-p gapped-OFDM, the M subcarriers $\{a_{N-M}, a_{N-M+1}, \ldots, a_{N-1}\}$ are compressed from the N subcarriers $\{S_0, S_1, \ldots, S_{N-1}\}$ by an $M \times N$ $(M \leq N)$ NODFT matrix $\boldsymbol{W}$ to keep the SE unchanged, where its (m, n)th entry is denoted by $W_{m,n} = \exp(-j2\pi mn/N)/\mathrm{sqrt}(M)$, for $m = 0, 1, \ldots, (M-1)$, and $n = 0, 1, \ldots, (N-1)$. Note that $\boldsymbol{W}$ is equivalent to the standard DFT matrix when $M = N$. Considering the mitigation of nonlinear distortion and the increase in SNR of residual subcarriers using the gap structure and the inter-carrier interference (ICI) induced by the non-orthogonal precoding and decoding [13], the value of M must be optimized to get the best transmission performance given one preset bias current. An inverse NODFT (INODFT) matrix $\boldsymbol{W}^{\mathrm{H}}$ is employed for decoding at the receiver side, which is the Hermitian transpose of $\boldsymbol{W}$.

A high PAPR limits the transmitter power efficiency, which is a crucial problem in an OFDM system. Figure 2(a) shows the complementary cumulative distribution function (CCDF) of the PAPR curves for different signals, indicating the significantly reduced PAPR provided by the proposed NODFT-p gapped-OFDM signal $(N-M = 12)$ when compared with the conventional OFDM case and DFT-spread OFDM $(N = M)$. It should be noted that $N-M = 12$ has been verified as the optimal gap width with a bias current of 80 mA in this work.

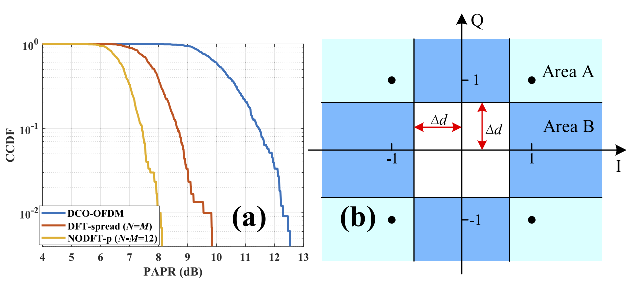

Fig. 2. (a) CCDF of PAPR for different signals, where 230/512 subcarriers are effectively modulated by QAM-4 symbols, and (b) mapping strategy of QAM-4 constellation in a CBID algorithm.

Since the matrix $\boldsymbol{W}$ and $\boldsymbol{W}^{\mathrm{H}}$ are no longer orthogonal, the ICI is purposely induced in the proposed scheme. The cascaded binary-phase-shift-keying iterative detection (CBID) [16] is an effective algorithm to mitigate the ICI based on the $N \times N$ correlation matrix $\boldsymbol{C} = \boldsymbol{W}^{\mathrm{H}}\boldsymbol{W}$, where the (i, k)th entry of $\boldsymbol{C}$ is given by

$$C_{i,k} = \sum_{m=0}^{M-1} \exp(-j2\pi m(k-i)/N)/M. \tag{1}$$

In the gth iteration of CBID, the received symbols $\boldsymbol{S}_g$ after the INODFT matrix decoding is first updated by

$$\boldsymbol{S}_g = \boldsymbol{R} + (\boldsymbol{I} - \boldsymbol{C})\boldsymbol{S}_{g-1}, \tag{2}$$

where $\boldsymbol{R}$ is the decoded symbols after the INODFT matrix, $\boldsymbol{I}$ is the identity matrix, and $\boldsymbol{S}_{g-1}$ represents the symbols after the $(g-1)$th iteration. As depicted in Fig. 2(b), the symbols inside areas A and B after the above iterations are mapped onto the corresponding constellation points, leaving other symbols unchanged until the next iteration. The threshold interval during the iteration is updated by $\Delta d = 1 - g/G$, where G is the preset total number of iterations.

The VNLE is also considered a useful nonlinear distortion compensation scheme. The output of the time-domain vth-order VNLE can be expressed as [17]

$$\begin{aligned} y[t] = & \sum_{l_1=0}^{L_1-1} h_1(l_1)x(t-l_1) + \sum_{l_1=0}^{L_2-1}\sum_{l_2=0}^{l_1} h_2(l_1,l_2)\prod_{\mu=1}^{2} x(t-l_\mu) \\ & + \sum_{l_1=0}^{L_3-1}\sum_{l_2=0}^{l_1}\sum_{l_3=0}^{l_2} h_3(l_1,l_2,l_3)\prod_{\mu=1}^{3} x(t-l_\mu) + \cdots \\ & + \sum_{l_1=0}^{L_v-1}\sum_{l_2=0}^{l_1}\cdots\sum_{l_v=0}^{l_{v-1}} h_v(l_1,l_2,\cdots,l_v)\prod_{\mu=1}^{v} x(t-l_\mu), \end{aligned} \tag{3}$$

where $x[t-l_\mu]$ is the $(t-l_\mu)$th sample of the received signal, $y[t]$ is the tth sample of the output signal after the VNLE, $h_v(l_1, l_2, \ldots, l_v)$ is the weighting coefficient of the vth order which is obtained by the $T/2$-spaced RLS algorithm in this work, and L_v is the memory length of the vth order kernel. As the nonlinear distortion in this work is mainly of the second order, only the diagonal terms of the third-order kernel are included in the third-order filtering to reduce the complexity, i.e., $l_1 = l_2 = l_3$ for the third-order kernels.

Then, we compared the computational complexity of the proposed NODFT-p gapped-OFDM with the $T/2$-spaced RLS-based third-order VNLE. For a fair comparison, we also considered the complexity required for updating the coefficients of the VNLE, i.e., the complexity of the time-domain $T/2$-spaced RLS algorithm, and the complexity of the frequency-domain zeros-forcing (ZF) equalizer. The RLS algorithm recursively finds the coefficients of the VNLE [18] in the training process at the receiver side, and this iterative process usually requires multiple iterations, i.e., $(N_{fft} + N_{cp})$ iterations required for each training OFDM symbol in this Letter, where N_{fft} is the size of IDFT used at the transmitter side to produce the real-valued signal, and N_{cp} is the length of cyclic prefix (CP) to combat CD. Based on [18], the required numbers of multiplications and additions for the time-domain $T/2$-spaced RLS algorithm in one iteration are $3L^2 + 2L + L_2(L_2+1) + 4L_3 + 1$, and $2L^2 + L + 1$, respectively, where $L = L_1 + L_2(L_2+1)/2 + L_3$, is the total tap number of the used third-order VNLE. As shown by Cheng *et al.* in Ref. [17], the corresponding input-output relationship of the VNLE can be expressed in the form of vector multiplication.

Table 1. Computational Complexity of Different Compensation Algorithms for One OFDM Symbol

	$T/2$-Spaced RLS-Based Third-Order VNLE		Proposed NODFT-p Gapped-OFDM Scheme	
	RLS	Third-Order VNLE	ZF Equalizer	CBID Algorithm
Multiplications/Symbol	$(N_{fft}+N_{cp})$ $(3L^2+3L+L_2(L_2+1)+4L_3+1)$	$(N_{fft}+N_{cp})$ $(L+L_2(L_2+1)+4L_3)$	M	$4GN^2+MN$
Additions/Symbol	$(N_{fft}+N_{cp})(2L^2+L+1)$	$(N_{fft}+N_{cp})(L-1)$	0	$3GN^2+7GN+(M-1)N$

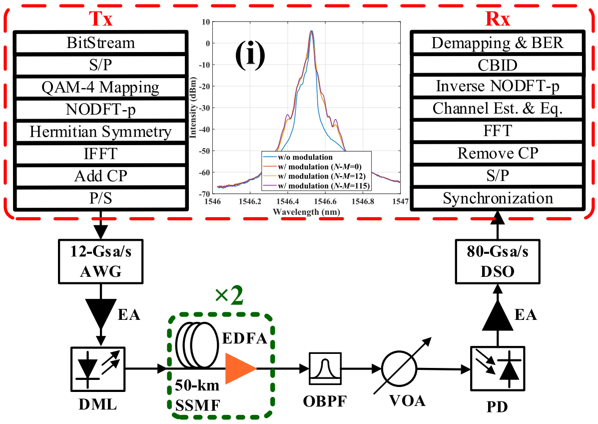

Fig. 3. Experimental setup and DSP of the proposed NODFT-p gapped-OFDM. (AWG: arbitrary waveform generator, EA: electrical amplifier, VOA: variable optical attenuator, PD: photodiode, DSO: digital oscilloscope). Inset (i): measured optical spectra under different modulation cases at BTB.

Then, the required numbers of multiplications and additions for the third-order VNLE when equalizing one OFDM symbol are $(N_{fft}+N_{cp})(L+L_2(L_2+1)+4L_3)$, and $(N_{fft}+N_{cp})(L-1)$, respectively. The ZF equalizer is a simple single-tap equalizer [19]. It does not need additions but needs M multiplications for finding channel coefficients or equalizing one OFDM symbol. The details of the CBID algorithm are described by Huang *et al.* in Ref. [16], and based on [16], the required numbers of multiplications and additions for the CBID algorithm when decoding one OFDM symbol are $4GN^2+MN$ and $3GN^2+7GN+(M-1)N$, respectively. Since both the proposed NODFT-p gapped-OFDM and the $T/2$-spaced RLS-based third-order VNLEs require the fast Fourier transform (FFT) algorithm at the receiver side to transform the time-domain signal into the frequency-domain, we ignore the complexity induced by this operation. Table 1 summarizes the required computational complexity of these two schemes.

Finally, we experimentally investigated the performance of the proposed scheme. Figure 3 shows the experimental setup and digital signal processing (DSP). At the transmitter, the bitstream after serial-to-parallel (S/P) conversion was first mapped onto QAM-4 symbols, which were allocated over 230 subcarriers ($N=230$), and then transformed into M subcarriers by the NODFT matrix. Hermitian symmetry was applied before performing a 512-point inverse fast Fourier transform (IFFT) to generate a real-valued signal. Then, a CP with a length of 16 was added to combat CD. To estimate the channel response and implement equalization at the receiver, 30 blocks of QAM-4 training sequences (TSs) were added before the 300 blocks of OFDM payload symbols. A 12-GSa/s arbitrary waveform generator (AWG) together with a DML at a center wavelength of 1546.2 nm converted the signal from the digital domain to

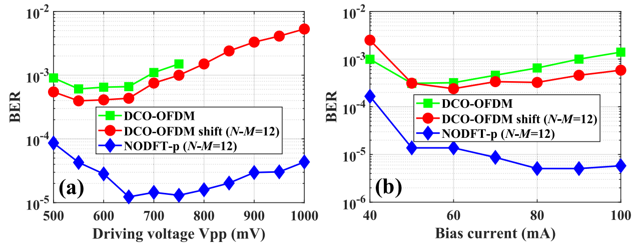

Fig. 4. BER performance as a function of (a) driving voltage Vpp, where the bias current was set to 80 mA, and (b) bias current, where Vpp was set to the corresponding optimum value.

the optical domain, where the threshold current of the DML was 11.2 mA. Therefore, the data rate of the signal was 9.5 Gb/s ($\approx$12G $\times$ 2bits $\times$ 230/512 $\times$ 512/528 $\times$ 300/330). After 100-km SSMF transmission, an optical bandpass filter (OBPF) was employed after the output of the second erbium-doped fiber amplifier (EDFA) to suppress the out-of-band amplified spontaneous emission noise. A variable optical attenuator (VOA) was used to vary received optical power (ROP) to evaluate the sensitivity curve. The signal was then detected by a 40-GHz photodiode (PD) and finally captured by a real-time oscilloscope operating at 80 GSa/s for offline DSP. It should be noted that the inherent driver of the DML is AC-coupled and the cutoff frequency of the bias tee is 10 MHz, which is comparable with the subcarrier spacing (6 GHz/230 $\approx$ 26.1 MHz). To reduce its influence on low-frequency subcarriers and keep the SE unchanged, we shifted two modulated subcarriers to high frequency in DCO-OFDM signals with and without the VNLE for a fair comparison.

In order to achieve a better transmission performance, both the driving voltage Vpp and the bias current of the DML were optimized under ROP = 1 dBm after 100-km transmission, as shown in Fig. 4. It can be observed from Fig. 4 that the optimal Vpps for the three schemes were 550 mV, 550 mV, and 650 mV, respectively, and the optimal bias currents were 50 mA, 60 mA, and 80 mA, respectively. These optimized parameters were used in this work. We set the DML's parameters in back to back (BTB) transmission the same as 100 km to observe the joint impact of chirp and dispersion in this work.

Figure 5(a) presents the SNR with respect to different $(N-M)$ values. We can see from Fig. 5(a) that the SNR increases with the increase in $(N-M)$, which is consistent with the analysis and results described by Nguyen *et al.* in Ref. [11]. This is because the nonlinear distortion mainly falls within the low-frequency band, and the gapped-OFDM makes it possible to avoid much of the distortion [11]. Besides, abandoning these subcarriers located at the low-frequency band with a low SNR is also helpful in alleviating the impairment. However, the ICI induced by the non-orthogonal precoding and decoding increases as the gap width increases [15], and it may also result in the loss of the subcarriers with a high SNR if the gap width is too large. Therefore,

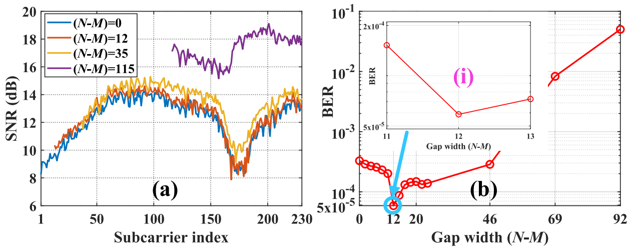

Fig. 5. (a) Calculated SNR after 100-km SSMF transmission, and (b) measured BER versus $(N-M)$, where the bias current is 80 mA. Inset (i): BER versus the value of $(N-M)$ around $N-M=12$.

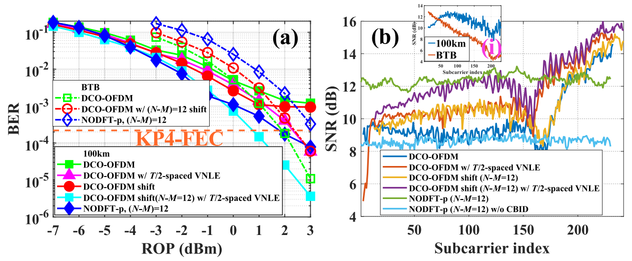

Fig. 6. (a) Measured ROP sensitivity curves, and (b) corresponding SNR curves after 100-km transmission at ROP = 1 dBm. Inset (i): measured SNR profiles of NODFT-p under BTB (orange) and after 100-km transmission (blue).

an optimal gap width exists to fully utilize the subcarriers that are suitable for data transmission.

Figure 5(b) depicts the impact of the gap width on the bit-error rate (BER) performance. The BER first decreases along with the growing gap width, thanks to the abandonment of the subcarriers with a low SNR due to nonlinear distortion. The BER then increases with the growing gap width because of the increased ICI and the sacrifice of subcarriers with a high SNR. The optimal gap width is obtained at $N-M=12$, corresponding to a ∼0.28-GHz bandwidth, and the corresponding optimal number of iterations G in CBID was set to 4.

Figure 6(a) shows the measured ROP sensitivity of the received signals. Herein, we have also studied the performance of shifting the modulated subcarriers directly to high frequency by the optimized gap width $(N-M)$ for comparison. The optimal tap number of the $T/2$ RLS-based third-order VNLE was (91, 16, 7). As shown in Fig. 6(a), for the case of 100-km SSMF transmission where there is higher nonlinear distortion generated by the interaction between chirp and CD, the DCO-OFDM with shifting using the VNLE performs best since it can avoid much nonlinear distortion distributed at a low frequency and eliminate the residual nonlinearity with the powerful VNLE. However, it should be noted that subcarrier shifting is not universally applicable considering the bandwidth limitation and the case when N is close to $N_{fft}/2$. Besides, the proposed scheme achieved ∼0.4-dB sensitivity improvement at the KP4-FEC threshold over the conventional DCO-OFDM using the VNLE. Based on the computational complexity analysis summarized in Table 1, the proposed scheme with the optimal gap width can reduce the computational complexity by 90% for multiplication, and 88.32% for addition compared to the schemes using the VNLE. For the BTB case, we can see that the proposed scheme with a gap at low frequency shows worse performance than that after SSMF transmission. This can be explained by the inset (i) of Fig. 6, where the BTB SNR has a frequency roll-off, but the performance of its high-frequency part is enhanced after SSMF transmission due to the interaction between chirp and CD [6]. That is why setting a gap at the low frequency only works in the 100-km case. Figure 6(b) presents the measured SNR curves of different schemes, indicating that the NODFT-p can spread the noise evenly over subcarriers and CBID can further improve the overall SNR.

In this Letter, we have proposed an NODFT-p gapped-OFDM scheme to mitigate the nonlinear distortion in a DML-based optical transmission system. In contrast to the conventional gapped-OFDM, the proposed scheme can reduce the nonlinear distortion without sacrificing the SE. The performance improvement and the computational complexity reduction of the proposed scheme have been experimentally verified when compared with the conventional VNLE scheme, both at the optimal setting. In conclusion, the proposed scheme is a promising technique to eliminate the nonlinear distortion in a DML-based system.

Funding. Research Grants Council, University Grants Committee (14205820).

Disclosures. The authors declare no conflicts of interest.

Data availability. Data underlying the results presented in this Letter are not publicly available at this time but may be obtained from the authors upon reasonable request.

REFERENCES

1. D. Qian, N. Cvijetic, J. Hu, and T. Wang, J. Lightwave Technol. **28**, 484 (2010).
2. M. A. Khalighi and M. Uysal, IEEE Commun. Surv. Tutorials **16**, 2231 (2014).
3. K. Zhong, X. Zhou, Y. Wang, T. Gui, Y. Yang, J. Yuan, L. Wang, W. Chen, H. Zhang, J. Man, L. Zeng, C. Yu, A.P. T. Lau, and C. Lu, in Proc. Opt. Fiber Commun. (2017), p. Tu2D.7.
4. L. Xue, L. Yi, and W. Hu, IEEE Photonics J. **10**, 7103508 (2018).
5. F. Gao, S. Zhou, X. Li, S. Fu, L. Deng, M. Tang, D. Liu, and Q. Yang, Opt. Express **25**, 7230 (2017).
6. C. Sun, S. H. Bae, and H. Kim, IEEE Photonics Technol. Lett. **29**, 130 (2017).
7. C. C. Wei, H. L. Cheng, and W. X. Huang, J. Lightwave Technol. **36**, 3502 (2018).
8. C. Sanchez, J. L. Wei, B. Ortega, and J. Capmany, J. Lightwave Technol. **31**, 3277 (2013).
9. D.-Z. Hsu, C.-C. Wei, H.-Y. Chen, W.-Y. Li, and J. Chen, Opt. Express **19**, 17546 (2011).
10. N. S. André, K. Habel, H. Louchet, and A. Richter, Opt. Express **21**, 26527 (2013).
11. H.-M. Nguyen, C.-C. Wei, C.-Y. Chuang, J. Chen, H. Taga, and T. Tsuritani, J. Lightwave Technol. **36**, 5617 (2018).
12. P. Song, Z. Hu, Y. Dai, and C. K. Chan, in Proc. of Optical Fiber Communication Conference (OFC) 2023, p. W2A.30.
13. Z. Hu and C. K. Chan, in Optical Fiber Communication Conference (Optical Society of America, 2020), p. M1J. 5.
14. K. Zhang, Q. Zhuge, H. Xin, W. Hu, and D. V. Plant, Opt. Express **26**, 34288 (2018).
15. Z. Hu and C.-K. Chan, J. Lightwave Technol. **38**, 632 (2020).
16. J. Huang, Q. Sui, Z. Li, and F. Ji, IEEE Photonics J. **8**, 7903709 (2016).
17. W. Cheng, M. Xiang, H. Yang, X. Huo, Y. Ma, J. Li, S. Fu, and Y. Qin, Opt. Lett. **48**, 351 (2023).
18. K. D. Bandara, P. Niroopan, and Y. Chung, J. Inst. Electron. Telecommun. Eng. **59**, 672 (2014).
19. X. Ouyang and J. Zhao, IEEE Commun. Lett. **18**, 1319 (2014).